Tilted potential induced coupling of localized states in a graphene nanoconstriction

M. R. Connolly,[1] K. L. Chiu,[1] A. Lombardo,[2] A. Fasoli,[2] A. C. Ferrari,[2] D. Anderson,[1] G. A. C. Jones,[1] and C. G. Smith[1]

[1]*Cavendish Laboratory, Department of Physics, University of Cambridge, Cambridge CB3 0HE, United Kingdom*

[2]*Department of Engineering, University of Cambridge, Cambridge CB3 OFA, United Kingdom*

(Received 10 September 2010; revised manuscript received 17 November 2010; published 23 March 2011)

We use the charged tip of a low-temperature scanning probe microscope to perturb the transport through a graphene nanoconstriction. Maps of the conductance as a function of tip position display concentric halos and, by following the expansion of the halos with back-gate voltage, we are able to identify an elongated domain over the nanoconstriction where they originate. Amplitude modulations of the transmission resonances are correlated with the gradient of the tip-induced potential and we analyze this in terms of modified tunnel coupling between localized states.

DOI: 10.1103/PhysRevB.83.115441 PACS number(s): 72.80.Vp, 81.07.Ta, 73.23.Hk, 85.35.Be

I. INTRODUCTION

The demand for materials capable of realizing the next generation of electronic and photonic devices continues to fuel interest in the electronic and optical properties of graphene.[1,2] The single-electron control offered by quantum dots makes them ideal test-beds for examining properties of Dirac quasiparticles such as the g factor,[3] excitation spectra,[4] and spin relaxation time.[5] A graphene quantum dot typically consists of an etched island that is tunnel coupled to large-area leads by ultranarrow (<30 nm) constrictions.[6,7] Broad and irregular modulations of the Coulomb blockade oscillations obtained from such structures have been attributed to disorder-induced dots within the constrictions themselves.[7] Although their size, spacing, and precise origin are currently unclear, at sub-30-nm length scales, it is likely that potential inhomogeneities and edge roughness play a role in creating these localized states.[8–10] The random transport properties associated with unintentional localization are not only problematic for analyzing quantum dot structures but also present challenges for the development of graphene nanoribbon electronics.[11] In contrast with large-area graphene sheets, whose on-off conductance ratio is too low for applications such as switches and transistors, narrow channels do exhibit a length- and width-dependent transport gap where the conductance is suppressed for a range of source-drain bias around the charge neutrality point.[10,12,13] However, this gapped region is larger than estimates based on confinement effects alone, and also exhibits sharp resonances at low temperature.[10,13,14] Hence the focus has recently shifted away from tailoring transport properties using edge lattice symmetries and more toward understanding the role of disorder.[12,15]

Transport through narrow graphene channels in the presence of disorder has been explored within different theoretical and semiempirical frameworks, including Anderson localization,[16] percolation models,[17] disorder- and edge-roughness-induced quantum dot formation,[10,13,15,18] and lateral confinement.[12] Since these mechanisms are partly distinguished by *where* localization occurs, local probes offer a powerful way to discriminate between them. In this work we use the charged tip of a scanning probe microscope to perturb the transport through a lithographically defined graphene nanoconstriction. By monitoring the conductance of the nanoconstriction as a function of tip position, we are able to detect the presence of multiple quantum dots within the channel via the effect of the potential from the tip.

II. EXPERIMENTAL METHOD

Our graphene flakes are mechanically exfoliated from natural graphite onto a highly doped Si substrate capped with a 300-nm-thick SiO_2 layer. Optical microscopy[19] and Raman spectroscopy[20] are used to locate the flakes and confirm that they are monolayers. Two Ti-Au contacts (of 10 and 50 nm thickness) were patterned using lift-off processing and a ≈90-nm-wide channel connected by tapered leads was etched using an O_2 plasma [Fig. 1(b)]. Figure 1(a) shows the conductance G of the device as a function of back-gate voltage V_{BG} applied to the Si substrate at $T = 8$ K. As expected,[7] G is strongly suppressed for a range (ΔV_{BG}) around the neutrality point ($V_{NP} \approx 12$ V) except for irregularly spaced resonances where G increases over a narrow range of V_{BG}. The density of resonances decreases at lower temperature while their line shape remains roughly constant [inset, Fig. 1(a)]. At larger source-drain voltage (V_{SD}), the conductance between the resonances increases, leading to diamond-shaped regions with ΔV_{SD} of 15–20 mV where the current is blockaded [Fig. 1(c)].

A schematic of our scanning gate microscopy (SGM) setup is shown in Fig. 1(b). To perform SGM, a current is driven through the device and its conductance is recorded while a sharp conducting tip is scanned in close proximity (<100 nm) over its surface.[21,22] To approach the sample at low temperature, we use a modified commercial scanning probe microscope head (AttoAFM I) mounted to the mixing chamber of a dilution refrigerator. The oscillation of the cantilever is measured using standard interferometric detection with a fiber-based infrared laser. By monitoring the response of the device at different laser powers, we eliminate the possibility of optical excitation arising from indirect illumination by the laser. We use a Pt-Ir–coated cantilever (NanoWorld ARROW-NCPt) with a nominal tip radius of 15 nm.

III. RESULTS AND DISCUSSION

A. Tapping-mode imaging

Figure 2(a) shows a typical SGM image[23] captured over the constriction in tapping mode with an applied tip bias

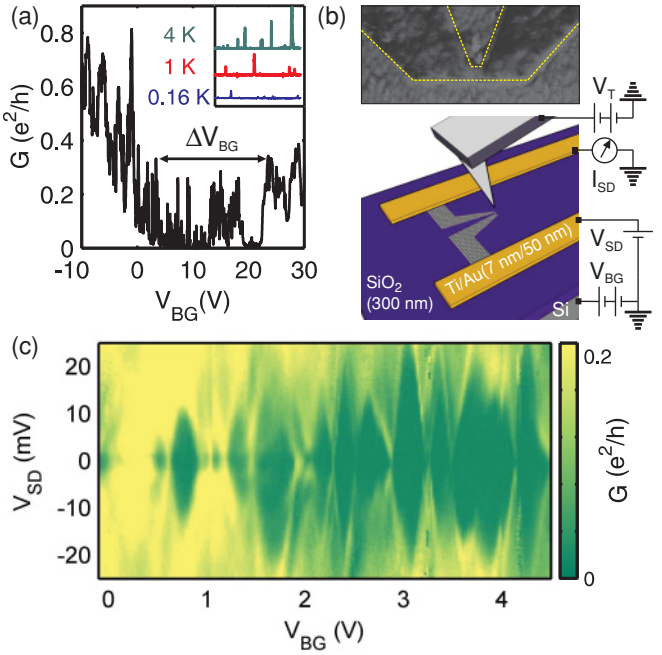

FIG. 1. (Color online) (a) Conductance of the nanoconstriction as a function of V_{BG} at $T = 8$ K ($V_{SD} = 5$ mV). Inset: Plots of the zero-bias conductance (excitation voltage 300 μV) within the transport gap ($V_{BG} = 7$–10 V) at different temperatures. (b) Setup used to perform scanning gate microscopy. Inset: Atomic force micrograph ($\approx 1 \times 0.5\ \mu m^2$) showing the 90-nm-wide constriction. (c) Conductance as a function of V_{SD} and V_{BG}. Diamonds of suppressed conductance at low V_{SD} indicate the presence of Coulomb blockaded islands with characteristic charging energy of ≈15–20 meV.

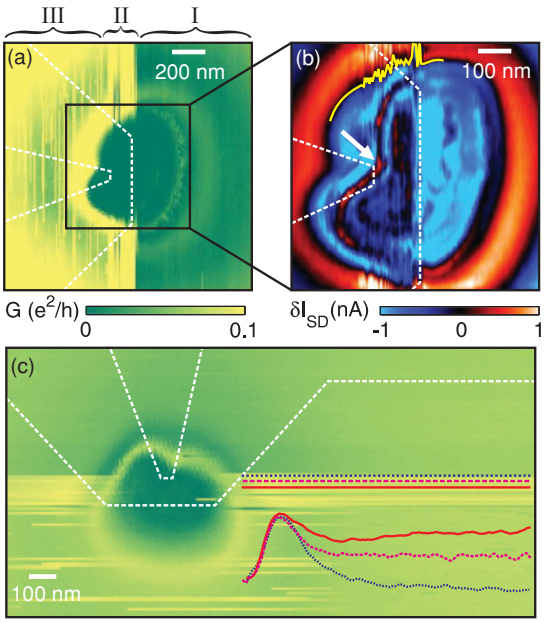

FIG. 2. (Color online) (a) Scanning gate image of the nanoconstriction captured in tapping mode ($V_T = 0.5$ V, $V_{BG} = 0$ V, $V_{SD} = 5$ mV). (b) Transconductance scanning gate image captured with an ac bias with peak-to-peak amplitude of $V_T = 100$ mV oscillating at 700 Hz. The arrow indicates the position of the indent used to align lift-mode scanning gate images. (c) Scanning gate image with same conditions as (a) illustrating the "locking" of the conductance at the approximate value it has after leaving the region over the nanoconstriction. Superimposed profiles show the conductance in the vicinity of the corresponding lines in the image. White dashed outlines indicate the edge of the nanoconstriction extracted from the simultaneously captured topographic image. We attribute the jumps in conductance observed in the left of image (a) and the lower half of image (c) to switching induced by the movement of trapped charges within the vicinity of the dot.

$V_T = 0.5$ V and $V_{BG} = 0$ V. Elongated halos alternating between enhanced and suppressed G encircle the constriction. Such features are typical of SGM on quantum dots, with each halo corresponding to the locus of points where the tip's contribution to the electrostatic potential of the dot is sufficient to overcome the Coulomb blockade.[21] In tapping mode there is an additional time dependence in the position of each halo due to the oscillating height of the tip. By analyzing the height dependence of the conductance as the tip is retracted directly over the constriction, we estimate that the amplitude of the cantilever oscillation (≈8 nm) produces an effective oscillation of V_T of ≈1 mV. Since this is small in comparison with the typical change in tip voltage required to sweep through a resonance (≈100 mV), we ignore the small broadening which arises in tapping mode. Note also that there is no response when the tip is over the leads on either side of the constriction. This excludes the possibility that direct conduction between the biased tip and the graphene contributes to the image contrast in tapping mode, probably because of the small tip-graphene contact area and the residual layer of polymethyl methacrylate (PMMA).

The halos are continuous in region I, but are broken by a stripe in region II where the tip crosses the graphene edge on either side. Although their elongated axis is still aligned with the channel in region III, the halos are indented where the inside edge of the constriction meets the tapered lead. This indent is highlighted in Fig. 2(b), which shows a SGM image captured under the same conditions as Fig. 2(a), but with a modulated bias applied to the tip.[24] The images of δI_{SD} produced in this mode show similar features to the dc-bias mode but with more halos, since each halo in the dc-bias image produces two halos of high contrast where the derivative ($|\partial I_{SD}/\partial V_T|$) on either side is a maximum. The modulated bias has the effect of enhancing the contrast over the constriction. The stripe in region II is clearly distinguished as a region where the conductance jumps over the constriction, and fluctuations appear in the position of the halo, as highlighted by the yellow line near the top of Fig. 2(b).

The stripe rotates with the scan direction and is always parallel to the fast-scan axis. A region with these properties was also observed in SGM of subsurface quantum dots,[25] where it was attributed to tip-induced rearrangements of charge in the vicinity of the dot. In our system it is likely that charge is deposited on the residual PMMA as the biased tip taps the area over the constriction. The deposited charge effectively offsets the electrostatic potential experienced by the localized states during each scan, leading to jumps in the signal over the constriction. The "locking" of the conductance at the value it has when the tip leaves the sensitive region in any fast-scan direction is also consistent with this picture: The deposited charge effectively maintains the potential contributed by the tip so that the transport becomes independent of tip position. Once

the tip ceases to scan directly over the constriction, the stripe is no longer observed, suggesting that the time for discharge is of the order of seconds. Further support for this is shown in Fig. 2(c), which shows a dc-mode image captured under the same conditions as Fig. 2(a). Typical line scans at different distances from the edge of the stripe are superimposed on the image and reveal that the locking of the conductance gradually diminishes as the tip leaves the region over the nanoconstriction. Note that the stripe matches the entire width of the constriction, suggesting that the localized states are distributed over the channel width.

There is good agreement between the origin of the halos and the topographic location of the constriction, presumably due to the proximity of the tip in tapping mode.[8] While tapping mode was useful for relating SGM structures to the underlying topography, it was unsuitable for continuous use, as the distribution of resonances in $G(V_{BG})$ could change between successive scans [note the difference between Figs. 2(a) and 2(c)]. To avoid this instability, we performed all subsequent scans in "lift mode," with the static tip ≈30 nm from the surface, and used the indent [arrow, Fig. 2(b)] as a reference point for overlaying the topographic outline.

B. Lift-mode imaging

To establish where the conductance halos originate, we park the biased tip ($V_T = 2$ V) over the channel and tune V_{BG} such that G lies between two resonances [Fig. 3(b)]. The first resonance manifests as the outer halo in image 1 of Fig. 3(a). With increasing V_{BG}, the second resonance emerges as a disordered domain, which is aligned with the channel and extends into the leads with weak and variable contrast [images 2–4, Fig. 3(a)]. Once G is tuned to the peak of the second resonance, the domain is roughly the same width as the channel and splits into a single halo [image 5, Fig. 3(a)]. Recent scanning gate images obtained over nanoconstrictions connected to a quantum dot exhibit similar features arising from localized states.[8] While the shape of the domain depends on the profile of the tip potential as well as the shape of the region of localized states,[26] tip-induced distortions seem to play less of a role here because the orientation, width, and location of the domain compare favorably with the constriction itself. We note, however, that the lever-arm of the tip-graphene system will reflect the geometric structure, making an unambiguous determination of the exact shape or position of the localized state difficult.

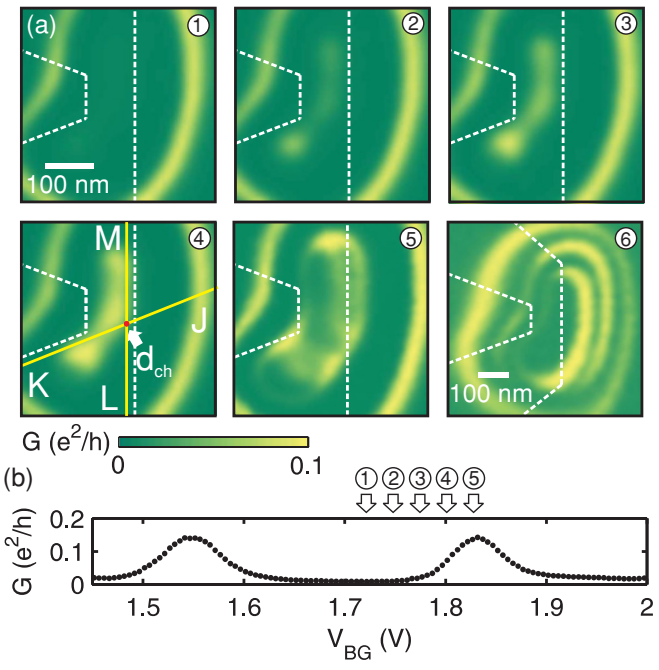

FIG. 3. (Color online) (a) Sequence of lift-mode scanning gate images (1–5) showing the evolution of the conductance halos with back-gate voltage ($V_T = 2$ V). Image 6 illustrates the typical left-right asymmetry in the amplitude of halos within this range of back-gate voltage. Dashed outline indicates the approximate location of the nanoconstriction. (b) Linear conductance as a function of back-gate voltage. Numbered arrows indicate the back-gate voltages at which the corresponding images in (a) were captured.

While the overlapping Coulomb diamonds and a reduction in the density of resonances at lower temperature (T) [inset, Fig. 1(a)] imply that localization is due to chargeable islands separated by tunnel barriers,[27] neither SGM mode reveals images with the characteristic signatures of multiple quantum dots, such as interlocking or anticrossing halos.[8,21,28] These observations are reconciled in the case of islands with insufficient capacitive coupling to create charging effects between them.[8] The latter may also reflect the elevated tunnel coupling (Γ) between the leads and the localized states in this region of V_{BG}, an interpretation supported by the T independence of the peak line shape, which suggests that $\hbar\Gamma > k_B T$. Furthermore, one would expect the effect of a broad tip potential to be similar to a global back gate if there are multiple islands which are closely spaced, leading to the concentric, rather than interlocking, halos seen in Fig. 3(a).

C. Tip-position-dependent amplitude modulations

In the absence of pronounced multiple-dot features in the shape of the halos, we focus on the tip-position-dependent amplitude modulations of the halos, such as those illustrated in image 6 of Fig. 3(a). This procedure is similar to that adopted in Ref. 8 for analyzing the capacitive coupling between a well-defined quantum dot and a localized state in the tunnel barrier. Here the tip-position-dependent amplitude modulations appear within one set of Coulomb halos, and are more likely related to the *tunnel* coupling between localized states, which are too close to give rise to two sets of Coulomb halos with spatially separated centers.

To analyze the spatial variation in the amplitude modulations more clearly, the tip was moved in 30-nm steps along the line JK in Fig. 3(a) and the back-gate voltage was swept at each point. (We analyze data taken along JK because it traverses the kinked area of the domain, although qualitatively the same behavior was observed for all lines running perpendicular to the channel.) The resulting $G(V_{BG},x)$ maps along JK are plotted in Fig. 4(a) at different tip voltages. First, we consider the shape of the curves. Figure 4(b) shows the set of $V_P(x)$ curves highlighted in Fig. 4(a) by overlaid lines, where V_P denotes the position of a resonance in back-gate voltage. These curves exhibit the expected dependence on tip voltage: For positive tip voltages, the electrostatic potential

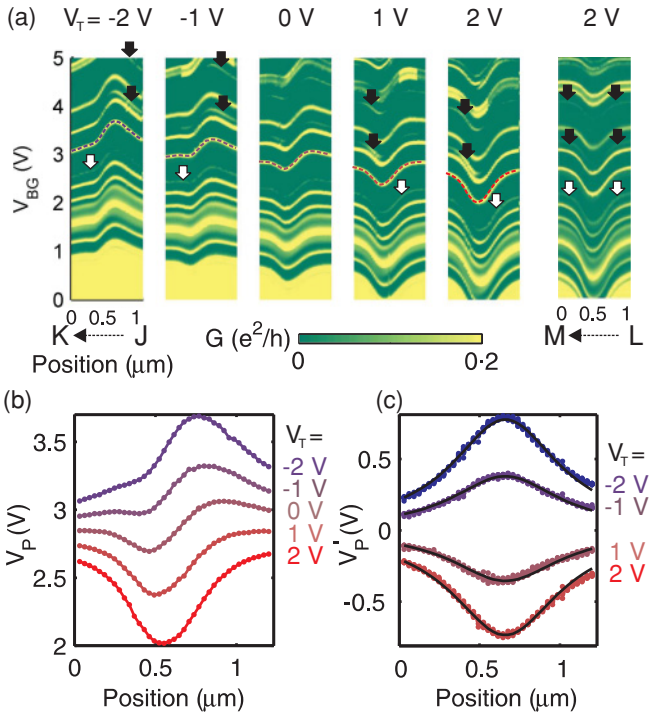

FIG. 4. (Color online) (a) Main: Linear conductance as a function of back-gate voltage and tip position along the line JK in Fig. 3 at different tip voltages. Arrows highlight resonances which exchange side upon reversing the sign of the tip potential. Right: The same measurement performed along the direction LM at $V_T = 2$ V. (b) Plots of the back-gate voltage V_P of the resonance overlaid by dashed lines in (a), as a function of position along JK at different tip voltages. (c) The same plot as (b) for nine of the resonances in (a) with the zero-V_T variation subtracted. Solid lines are fitted Lorentzians.

on the constriction increases as the tip approaches, leading to a shift in $V_P(x)$ to lower back-gate voltage, while the opposite is the case for negative tip voltages. We attribute the variation of V_P at zero applied V_T to a combination of screening, contact potential difference, charged debris on the tip, and capacitive coupling between the tip and the back gate.[26,28,29] Note that the symmetry of V_P in Fig. 4(a) improves in the range of V_T and V_{BG} where the images in Fig. 3(a) were captured, supporting our previous assertion that zero-V_T distortions are minimized. The asymmetry in the shape of $V_P(x)$ upon exchanging tip polarity masks the tip-voltage-dependent component of the tip-graphene interaction. By subtracting from each V_P its behaviour at $V_T = 0$ V, however, we obtain a set of corrected data, $V'_P(x)$, which are symmetrical and well fitted by Lorentzians given by $V'_P = A/[4(x - d_{ch})^2 + w^2]$, where d_{ch} is the center of the Lorentzian along JK [indicated in Fig. 3(a)], w is its full-width half maximum, and $A \approx \beta V_T$, with $\beta \approx 0.38 \pm 0.01$. We find that $d_{ch} \approx 675 \pm 10$ nm and $w \approx 805 \pm 20$ nm for thirty-six curves corresponding to nine of the resonances in Fig. 4(a). The value of w is in good agreement with the width of tip-induced potentials reported previously.[29,30] Considering the radius of curvature of the tip apex, the surprisingly low spatial resolution obtained here suggests that the long-range "gating effect" from the tip cone dominates at these lift-mode heights (see Ref. 31 for a discussion of this effect). We note that recent SGM experiments on magnetic-field-induced localized states in two-dimensional electron systems have achieved spatial resolutions better than 150 nm at lift heights of ≈50 nm.[32] While this is still poor in comparison with the dimensions of the tip apex, it is likely that the screening ability of planar systems leads to a sharper effective potential profile experienced by the localized state, as well as a lift-height dependence of the spatial resolution. Based on this, we suggest that the device geometry, rather than the lift height or shape of the tip, is the limiting factor in resolving localized states in graphene nanostructures using SGM. This is supported by other SGM images of graphene nanostructures captured at a lift height of ≈40 nm, which also do not show a dramatic enhancement of the spatial resolution over the range 150–40 nm.[8]

We now consider the mechanism for amplitude modulations which gives rise to the left-right asymmetry of the halos in image 6 of Fig. 3(a). Such halos correspond to the resonances highlighted by arrows in Fig. 4(a). Figure 4(a) reveals a particularly striking dependence of these resonances on the polarity of the tip voltage: The maximum conductance G_{Max} of the resonances highlighted by black arrows in Fig. 4(a) is enhanced (suppressed) when the tip is closer to K (J) for $V_T = 2$ V, while the opposite behavior is observed upon reversing the side and sign of the tip potential. By contrast, no such asymmetry is observed if the same measurement is performed with the tip stepped parallel to the channel [LM in Fig. 3(a)]. Since exchanging both the side and sign of the tip potential along JK preserves the in-plane electric field direction perpendicular to the channel, i.e., $E(-x) = -E(x)$, the observed asymmetry is naturally described in terms of the tilted potential induced across the channel.

Figure 5(a) shows line plots of $G(V_{BG})$ around the pair of resonances indicated by the lower black arrow in Fig. 4(a). We find that the maximum modulation of both resonances is reached when the tip is between the center of the channel and point K. This is precisely where the gradient ($\Delta V'_P$) of the corrected tip-induced potential is at maximum. Since the latter can be related to the in-plane component of the electric field by $E \propto \Delta V'_P/\Delta x$, this is further evidence that the electric field controls the amplitude of the resonance. This dependence is shown explicitly in Fig. 5(b), where we plot the maximum conductance (G_{Max}) of peak 2 as a function of $\Delta V'_P$. The data is well described by an exponential function, $G_{\mathrm{Max}} \approx e^{-\Delta V'_P/\gamma} + D$, where $D \approx 0.01\, e^2/h$ accounts for the nonzero conductance floor and $\gamma \approx 0.02$ V. The reason why the data is well described by the corrected rather than the raw potential may be due to the fact that the indirect tip-position-dependent changes in potential, such as the screening of electric fields from the environment, occur uniformly across the constriction and therefore only shifts the position of each resonance in the back-gate. At lower tip voltages, the influence of the bias-independent effect of the tip is also much larger, and G_{Max} is no longer simply related to $\Delta V'_P$.

Similar behavior is observed by the other resonance highlighted by the black arrow in Fig. 4(a), and the opposite behavior is observed for the resonance indicated by the white arrow. Such variations in G_{Max} are usually ascribed to tip-induced modulations in the tunnel barriers, and are

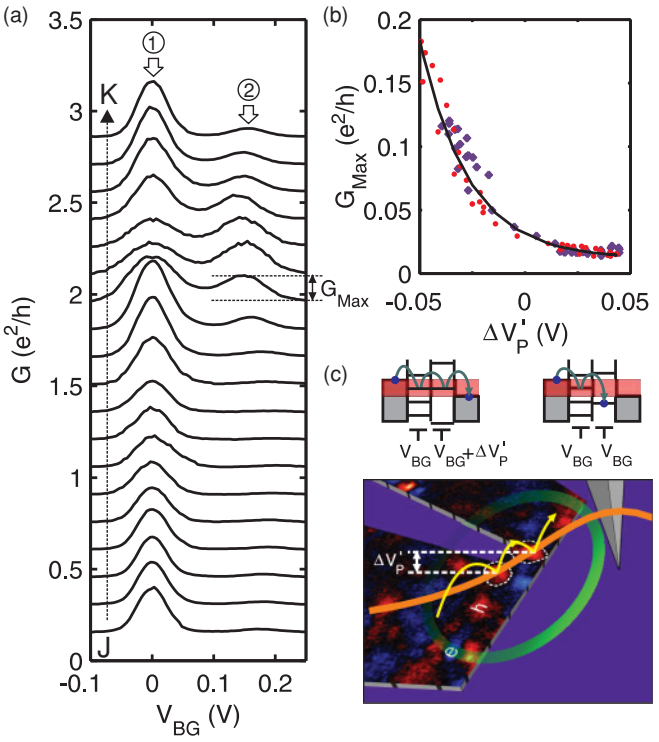

FIG. 5. (Color online) (a) Conductance as a function of back-gate voltage with the tip at different positions along JK in Fig. 3(a) with $V_T = 2$ V. Each curve has been vertically offset for clarity and horizontally offset such that peak (1) is at $V_{BG} = 0$ V. (b) Maximum conductance of resonance (2) as a function of the gradient of the corrected tip-induced potential for data taken with $V_T = 2$ V (circles) and -2 V (diamonds). Solid line is an exponential fit using both data sets. (c) [Top] Schematic depictions showing the effect of the potential offset in the ladder of states of two dots. [Bottom] Cartoon depicting the proposed mechanism for amplitude modulations of the Coulomb halos. Around the charge neutrality point, electron (blue) and hole (red) puddles within the constriction form quantum dots (white dashed outlines) separated by tunnel barriers. In the case depicted the potential from the tip (orange solid line) aligns the states in the two dots, increasing the conductance of the halo to the right side of the constriction [c.f. Image 6, Fig. 3(a)].

therefore equally compatible with single-dot behavior.[34] The exponential dependence on $\Delta V'_P$ is moreover highly suggestive of tunnel barrier modulation. However, in light of the multiple-dot behavior exhibited in the transport data, we consider an alternative scenario. The different charging energies and coupling between the back gate and the dots within the channel should lead to a random distribution of resonances in $G(V_{BG})$, as a dot with the weakest coupling to the back gate modulates the amplitude of resonances from the more strongly coupled dot(s).[35,36] The tilted potential introduced by the tip effectively offsets the ladder of charge states in the dots relative to one another [Fig. 5(c)]. As a result, the alignment of states in different dots either increases [peak 2 in Fig. 5(a)] or decreases [peak 1 in Fig. 5(a)], and resonance is indicated by the white arrow in Fig. 4(a)], depending on their initial detuning. While it is not possible to extract the exact size of the dots from our measurements, this picture requires at least two dots to fit laterally within a constriction with width 90 nm, and is therefore consistent with the estimate (≈20–30 nm) extracted from recent scanning gate images,[8] as well as the measured charging energy of 10–15 meV.[12]

IV. CONCLUSION

We investigated the response of a graphene nanoconstriction to the local electrostatic potential of a scanning probe tip. In weakly invasive tapping mode, we observe jumps in the conductance when the tip scans over the constriction, suggesting that localization in graphene nanostructures is sensitive to the electrostatic environment produced by locally deposited charge. In lift mode, we observe the expansion of a single elongated conductance halo around the nanoconstriction, in agreement with the results presented in Ref. 8. Transport data combined with scanning gate measurements, taken at different tip potentials and positions, allow us to detect the presence of multiple dots within the constriction via tip-induced amplitude modulations of the resonances. We interpret the absence of halos with different centers to imply that the localized states within the constriction are too small to be spatially resolved with our scanning gate microscopy setup. Finally, we note that similar amplitude modulations in halos have been reported in previous SGM work on GaAs-based subsurface quantum dots.[34] Since we are able to relate them to the strength and direction of the electric field from the tip, the present work also provides an insight into the tip-dot interaction which occurs in scanning gate microscopy of quantum dot systems.

ACKNOWLEDGMENTS

This work was financially supported by the European GRAND project (ICT/FET). ACF acknowledges funding from the European Research Council Grant NANOPOTS, the EU Grants RODIN and Marie Curie ITN-GENIUS (PITN-GA-2010-264694), EPSRC Grant EP/G042357/1, and a Royal Society Wolfson Research Merit Award.

[1] A. K. Geim and K. S. Novoselov, Nature Mater. **6**, 183 (2007).
[2] F. Bonaccorso, Z. Sun, T. Hasan, and A. C. Ferrari, Nature Photonics **4**, 611 (2010).
[3] J. Guttinger, T. Frey, C. Stampfer, T. Ihn, and K. Ensslin, Phys. Rev. Lett. **105**, 116801 (2010).
[4] F. Molitor *et al.*, Europhys. Lett. **89**, 67005 (2010).
[5] M. R. Buitelaar, J. Fransson, A. L. Cantone, C. G. Smith, D. Anderson, G. A. C. Jones, A. Ardavan, A. N. Khlobystov, A. A. R. Watt, K. Porfyrakis, and G. A. D. Briggs, Phys. Rev. B **77**, 245439 (2008).
[6] L. A. Ponomarenko, F. Schedin, M. I. Katsnelson, R. Yang, E. W. Hill, K. S. Novoselov, and A. K. Geim, Science **320**, 356 (2008).

[7]C. Stampfer, J. Guttinger, F. Molitor, D. Graf, T. Ihn, and K. Ensslin, Appl. Phys. Lett. **92**, 012102 (2009).
[8]S. Schnez, J. Guttinger, M. Huefner, C. Stampfer, K. Ensslin, and T. Ihn, Phys. Rev. B **82**, 165445 (2010).
[9]C. Stampfer, J. Guttinger, S. Hellmuller, F. Molitor, K. Ensslin, and T. Ihn, Phys. Rev. Lett. **102**, 056403 (2009).
[10]K. Todd, H.-T. Chou, S. Amasha, and D. Goldhaber-Gordon, Nano Lett. **9**, 416 (2009).
[11]Z. Chen, Y. M. Lin, J. Rooks, and P. Avouris, Physica E **40**, 228 (2007).
[12]M. Y. Han, B. Ozyilmaz, Y. Zhang, and P. Kim, Phys. Rev. Lett. **98**, 206805 (2007).
[13]F. Molitor, A. Jacobsen, C. Stampfer, J. Guttinger, T. Ihn, and K. Ensslin, Phys. Rev. B **79**, 075426 (2009).
[14]X. Liu, J. B. Oostinga, A. F. Morpurgo, and L. M. K. Vandersypen, Phys. Rev. B **80**, 121407 (2009).
[15]M. Y. Han, J. C. Brant, and P. Kim, Phys. Rev. Lett. **104**, 056801 (2010).
[16]M. Evaldsson, I. V. Zozoulenko, H. Xu, and T. Heinzel, Phys. Rev. B **78**, 161407 (2008).
[17]S. Adam, S. Cho, M. S. Fuhrer, and S. Das Sarma, Phys. Rev. Lett. **101**, 046404 (2008).
[18]F. Sols, F. Guinea, and A. H. Castro Neto, Phys. Rev. Lett. **99**, 166803 (2007).
[19]C. Casiraghi, A. Hartschuh, E. Lidorikis, H. Qian, H. Harutyunyan, T. Gokus, K. S. Novoselov, and A. C. Ferrari, Nano Lett. **7**, 2711 (2007).
[20]A. C. Ferrari, J. C. Meyer, V. Scardaci, C. Casiraghi, M. Lazzeri, F. Mauri, S. Piscanec, D. Jiang, K. S. Novoselov, S. Roth, and A. K. Geim, Phys. Rev. Lett. **97**, 187401 (2006).
[21]M. T. Woodside and P. L. McEuen, Science **296**, 1098 (2002).
[22]M. A. Topinka, B. J. LeRoy, S. E. J. Shaw, E. J. Heller, R. M. Westervelt, K. D. Maranowski, and A. C. Gossard, Science **289**, 2323 (2000).
[23]I. Horcas, R. Fernandez, J. M. Gomez-Rodriguez, J. Colchero, J. Gomez-Herrero, and A. M. Baro, Rev. Sci. Instrum. **78**, 013705 (2007).
[24]M. R. Connolly, K. L. Chiou, C. G. Smith, D. Anderson, G. A. C. Jones, A. Lombardo, A. Fasoli, and A. C. Ferrari, Appl. Phys. Lett. **96**, 113501 (2010).
[25]A. Pioda, S. Kicin, T. Ihn, M. Sigrist, A. Fuhrer, K. Ensslin, A. Weichselbaum, S. E. Ulloa, M. Reinwald, and W. Wegscheider, Phys. Rev. Lett. **93**, 216801 (2004).
[26]S. Kicin, A. Pioda, T. Ihn, M. Sigrist, A. Fuhrer, K. Ensslin, M. Reinwald, and W. Wegscheider, New J. Phys. **7**, 185, 1367 (2005).
[27]A. Dorn, T. Ihn, K. Ensslin, W. Wegscheider, and M. Bichler, Phys. Rev. B **70**, 205306 (2004).
[28]A. C. Bieszynski, F. A. Zwanenburg, R. M. Westerwelt, A. L. Roest, E. P. A. M. Bakkers, and L. P. Kouwenhoven, Nano Lett. **7**, 2559 (2007).
[29]A. E. Gildemeister, T. Ihn, M. Sigrist, K. Ensslin, D. C. Driscoll, and A. C. Gossard, Phys. Rev. B **75**, 195338 (2007).
[30]N. R. Wilson and D. H. Cobden, Nano Lett. **8**, 2161 (2008).
[31]M. G. Pala, B. Hackens, F. Martins, H. Sellier, V. Bayot, S. Huant, and T. Ouisse, Phys. Rev. B **77**, 125310 (2008).
[32]B. Hackens, F. Martins, S. Faniel, C. Dutu, H. Sellier, S. Huant, M. Pala, L. Desplanque, X. Wallart, and V. Bayot, Nat. Commun. **1**, 39 (2010).
[33]Z. H. Ni, T. Yu, Z. Qiang, Y. Y. Wang, L. Liu, C. P. Wong, J. Miao, W. Huang, and Z. X. Shen, ACS Nano **3**, 569 (2009).
[34]P. Fallahi, A. C. Bleszynski, R. M. Westervelt, J. Huang, J. D. Walls, E. J. Heller, M. Hanson, and A. C. Gossard, Nano Lett. **5**, 223 (2005).
[35]I. M. Ruzin, V. Chandrasekhar, E. I. Levin, and L. I. Glazman, Phys. Rev. B **45**, 13469 (1992).
[36]P. Gallagher, K. Todd, and D. Goldhaber-Gordon, Phys. Rev. B **81**, 115409 (2010).